Reduction of bundle sheath size boosts cyclic electron flow in C_4 *Setaria viridis* acclimated to low light

Chandra Bellasio[a, b*], Maria Ermakova[b]

[a] Department of Biology, University of the Balearic Islands, 07122 Palma, Illes Balears, Spain.
[b] Centre of Excellence for Translational Photosynthesis, Research School of Biology, The Australian National University, Acton, Australian Capital Territory 2601, Australia.
[*] Correspondence: Chandra Bellasio (chandra.bellasio@uib.es)

Abstract

When C_4 leaves are exposed to low light, CO_2 concentration in the bundle sheath (BS) cells decreases, causing an increase in photorespiration relative to assimilation, and a consequent reduction in biochemical efficiency. These effects can be mitigated by complex acclimation syndromes, which are of primary importance for crop productivity, but not well studied. We unveil an acclimation strategy involving regulation of electron transport processes. Firstly, we characterise anatomy, gas-exchange and electron transport of C_4 *Setaria viridis* grown under low light. Through a purposely developed biochemical model, we resolve the photon fluxes and reaction rates to explain how the concerted acclimation strategies sustain photosynthetic efficiency. Our results show that a smaller BS in low light-grown plants limited leakiness (the ratio of CO_2 leak rate out of the BS over the rate of supply via C_4 acid decarboxylation) but sacrificed light harvesting and ATP production. To counter ATP shortage and maintain high assimilation rates, plants facilitated light penetration through the mesophyll and upregulated cyclic electron flow in the BS. This shade tolerance mechanism based on optimisation of light reactions is potentially more efficient than the known mechanisms involving the rearrangement of carbon metabolism, and can potentially lead to innovative strategies for crop improvement.

Keywords:

C_4 photosynthesis, Kranz anatomy, light harvesting, bundle sheath, light reactions, carbon reactions, NADP-ME, gas-exchange, modelling

Significance [max 75 words, 2 sentences]:

We mechanistically link the optical cross-section of leaf compartments with the rate of electron transport, the engagement of cyclic electron flow, the relative rate of ATP and NADPH generation, and fluxes through the carbon metabolism. The striking capacity of *Setaria viridis* to counter the decrease in light absorption in the bundle sheath with an increase of cyclic electron flow presents perhaps the most efficient mechanism of shade acclimation.

Introduction

Leaves of the majority of C_4 plants are organised in concentric cylinders: an external tube of mesophyll (M) cells surrounds a tube of bundle sheath (BS) cells, which are wrapping the innermost vasculature (Figure 1). This spatial arrangement imposes that light and CO_2 entering C_4 leaves pass through M cells before reaching the BS. CO_2 is hydrated to HCO_3^- by carbonic anhydrase in the M cytosol and then fixed by PEP carboxylase (PEPC) into C_4 acids, which may be transaminated or chemically reduced. C_4 acids diffuse to BS cells where they are decarboxylated either primarily by NADP-malic enzyme (NADP-ME), NAD-malic enzyme (NAD-ME), PEP carboxykinase (PEPCK), or by a combination of these. Decarboxylation provides higher CO_2 partial pressure at the site of ribulose 1,5-bisphosphate carboxylase/oxygenase (Rubisco) thereby largely suppressing the competitive reaction with oxygen leading to the wasteful process of photorespiration (von Caemmerer and Furbank, 2003, Bellasio *et al.*, 2014). For this function, C_4 photosynthesis is also referred to as biochemical carbon concentrating mechanism (CCM). Pyruvate resulting from the C_4 acids decarboxylation diffuses back to M cells where it is regenerated into PEP by pyruvate orthophosphate dikinase (PPDK) using 2 ATP molecules. Some of the CO_2 released in BS cells diffuses out to M cells (called leakage) which incurs in an additional ATP cost of C_4 photosynthesis (Farquhar, 1983, Henderson *et al.*, 1992, Bellasio and Griffiths, 2014a).

C_4 photosynthesis is highly sensitive to limiting light intensities. Under low irradiance, ATP and NADPH generation slows down, limiting both the reductive pentose phosphate cycle (RPP) and the C_4 cycle. Since activities of RPP and the C_4 cycle are tightly balanced (Kromdijk *et al.*, 2014) through light-regulation (Bailey *et al.*, 2007), a slowdown of C_4 acids diffusion into the BS inevitably results in a decrease of CO_2 concentration in BS cells (C_{BS}). Consequently, the ratio between CO_2 and O_2 concentration at the active sites of Rubisco decreases, favouring oxygenation over carboxylation, lowering the biochemical efficiency [ATP per gross assimilation of CO_2] of C_4 photosynthesis (Furbank *et al.*, 1990, Ubierna *et al.*,

2013)]. In crop canopies, where up to 50 % of net CO_2 uptake is fixed by shaded leaves, (Baker *et al.*, 1988, Long, 1993) light limitation plays an important role in decreasing canopy productivity (Kromdijk *et al.*, 2010), and understanding acclimation strategies of C_4 metabolism to light limitation is critical to increase crop production to meet the raising food and fodder demand (Evans *et al.*, 1991, Bellasio and Griffiths, 2014a).

Shading limits C_4 photosynthesis also at the cell level. M and BS cells both need light to power photosynthesis. The amount of light that can be harvested by the BS cell is limited by their size [precisely by the BS optical cross section (Bellasio and Lundgren, 2016)], by light absorption in the M [because of the concentric organisation, BS cells are in effect shaded, meaning that light harvesting in the M reduces the light available to reach BS cells (Kramer and Evans, 2011)], and depends on light quality. Green light is not strongly absorbed by chlorophyll, meaning that it can easily reach the BS, while blue light is all taken up by the upper chloroplasts and preferentially excites M cells (Evans *et al.*, 2007). M cells use light to produce ATP and NADPH through linear electron flow (LEF) engaging both photosystems (PS) while BS cells of NADP-ME plants are thought to produce mainly ATP through cyclic electron flow (CEF) around PSI. In this way, the relative absorption of excitation energy will influence the availability of ATP and NADPH. Bellasio and Griffiths (2014c) proposed that these environmentally driven shifts in ATP and NADPH production can be countered by adjusting ATP and NADPH consumption by carbon metabolism, with a surprising degree of flexibility – but only up to a defined limit, ultimately determining how the biochemical work is apportioned between the two cell types. However, the possibility that plants could respond to shift in energy availability by rearranging light reactions, in such a way that also the production of ATP and NADPH is regulated, received little attention.

We have recently shown that the photosynthetic apparatus of *Setaria viridis,* a model C_4 plant of NADP-ME subtype, rearranges in response to low light in a cell-specific fashion, preferentially increasing electron transport capacity in BS cells (Ermakova *et al.*, 2021b). We hypothesized that this was a response to a shortage of ATP in the BS, which could depend either on an increased consumption from dark reactions, or on a lower rate of production caused by a shortage of light. Here we resolve these drivers and their causal relationship. First, we measure anatomical properties of leaves from *S. viridis* grown under high light (HL) and low light (LL) and estimate how these would influence light harvesting of the M and the BS. Then, we conduct a comprehensive gas exchange characterisation under ambient and low O_2, with concurrent determination of PSII and PSI effective quantum yields, to estimate biochemical parameters and conductance to CO_2 diffusion at the M/BS interface (g_{BS}). Finally, we develop

a model integrating two electron transport chains with the light-harvesting properties of M and BS to study how the apportioning of light and carbon metabolism shifts in LL plants, and how these changes affect biochemical efficiency. We demonstrate that the decreased light interception in BS cells is effectively counteracted by an increase of CEF, uncovering another important link between biochemical properties and structural characteristics of C_4 leaves.

Methods

Plants

S. viridis plants (A10 ecotype) were grown in 2 L pots filled with commercial soil mix (Debco, Tyabb, Australia) supplemented with 1 g L^{-1} of slow release fertilizer (Osmocote, Scotts, Bella Vista, Australia). Plants were grown in controlled chambers with 28°C day, 24°C night, 60 % humidity, and 16 h illumination at the intensity of 1000 µmol m^{-2} s^{-1} or 300 µmol m^{-2} s^{-1} provided by halogen incandescent lamps (42 W, 2800 K, warm white, clear glass, 630 lumens, CLA, Brookvale, Australia) and Pentron Hg 4 ft fluorescent tubes (54 W, 4100 K, cool white, Sylvania, Wilmington, MA, USA), and reached by hanging a shade cloth above some of the plants. Growth light spectra are shown in Figure S2. All measurements were performed on the youngest fully expanded leaves sampled before flowering between 15 and 25 days after germination.

Leaf anatomy

Resin–embedded cross–sections were prepared and imaged according to Pengelly *et al.* (2010). Quantification of anatomical parameters was performed using Image J software (NIH, WI) on an equal number of secondary and tertiary veins as described in Bellasio and Lundgren (2016). Calculations of the M surface area exposed to the intercellular airspace (S_m) and the BS surface area per unit of leaf area (S_b) were made as described in Pengelly *et al.* (2010) using the curvature correction factor of 1.43 from Evans *et al.* (1994). Apparent absorbance was calculated as the log10 of the ratio between the luminance of background divided by the luminance of the tissue, both processed with Image J as described in Bellasio and Lundgren (2016) and averaged over two regions for n=6 replicates. Leaf absorptance was the complement to one of leaf reflectance and transmittance, both measured with a Li-Cor 1800-12 (Li-Cor, Lincoln, NE) integrating sphere, coupled to a Li–190S light sensor, following the manufacturer's instructions for calibration and calculations.

Chlorophyll

Total chlorophyll was extracted from frozen leaf discs ground using TissueLyser II (Qiagen, Venlo, The Netherlands) in 80% acetone, buffered with 25 mM 4-(2-hydroxyethyl)-1-piperazineethanesulfonic acid (Hepes)-KOH (pH 7.8). Chlorophyll *a* and *b* content was measured at 750 nm, 663.3 nm and 646.6 nm, and calculated according to Porra *et al.* (1989). The fraction of total leaf chlorophyll in BS cells was determined from the Chlorophyll *a*/*b* ratios leaves, BS and M cells as described in Ermakova *et al.* (2021b).

Western blotting and immunolocalization

Protein isolation from leaves, gel electrophoresis and western blotting were performed as described in Ermakova *et al.* (2019). PEPCK antibodies (Agrisera, Vännäs, Sweden) were used according to the manufacturer's protocol.

Immunodetection of PPDK on lightly fixed leaf cross-section was performed according to (Ermakova *et al.*, 2021a). Sections were treated with 1:100 PPDK primary antibody (Karki *et al.*, 2020), 1:200 Alexa Fluor 488–conjugated goat anti-rabbit secondary antibody (Life Technologies, Eugene, OR) and 0.05 % calcofluor white to stain cell walls. Fluorescence signal was captured with the Leica DM5500 microscope (Leica, Wetzlar, Germany) equipped with the Leica DFC7000T camera using the Leica Application Suite 4.12 software. Fluorescence was detected at 505–565 nm for PPDK (excitation 490–510 nm, YFP Filter Cube, Leica) and at 450–490 nm for cell walls (excitation 330–370 nm, A4 Filter Cube, Leica).

Simultaneous gas exchange, chlorophyll fluorescence and P700 measurements

Gas exchange, fluorescence and $P700^+$ absorbance changes were measured simultaneously with the setup of Bellasio and Farquhar (2019) on $n = 3$ biological replicates. Briefly, a portable gas exchange system (LI6400XT, Li–Cor) was modified to operate at low CO_2 concentrations (see licor.com) and fitted with a 6400–06 PAM2000 adapter (courtesy of Susanne von Caemmerer), holding a fibre probe in the upper leaf cuvette distant enough to minimise shading. Leaves were aligned without overlapping their edges to fill the cuvette. Light was provided by a bespoke red–blue light source, regulated to provide circa 90% red and 10% blue light, positioned to illuminate the leaf uniformly. Light intensity was measured through an in–chamber Gallium arsenide photodiode, calibrated using a Li–250 light sensor (Li–Cor). Neoprene gaskets were used on both sides of the cuvette. A mixture of 2 % O_2 was prepared by mixing ambient air and N_2 with a bespoke gas mixing unit (kindly assembled by Suan Chin

Wong). This mix of ambient air was CO_2–scrubbed with soda lime and humidified to a dew point of 15–17 °C upstream of the inlet to maintain water vapour pressure deficit around 1 kPa. CO_2 was added from a large cylinder (BOC, St Peters, Australia), using the CO_2 injection unit of the LI6400XT. Mass flow leaks (Boesgaard *et al.*, 2013) were monitored with a gas flow meter as detailed in Bellasio *et al.* (2016b).

PSII and PSI yields were measured with a Dual PAM–F (Heinz Walz GmbH, Effeltrich, Germany, courtesy of Dean Price). PSII activity was assessed with the pulse amplitude modulated fluorescence method using 620 nm measuring light of 9 µmol m^{-2} s^{-1} (Schreiber *et al.*, 1986). The redox state of P700, the reaction centre of PSI, was assessed by detecting absorbance of the cation at 830 nm with a dual wavelength (830/875 nm) unit, following the method of Klughammer and Schreiber (1994). Saturating pulses of red light (635 nm) at 20,000 µmol m^{-2} s^{-1} were used. First, P_M, the maximal level of $P700^+$, was recorded upon the application of a saturating pulse on top of the far-red light, and P_0, the minimal $P700^+$ signal, was recorder after that saturating pulse. Photosynthetic parameters (P, the steady-state $P700^+$ signal; P_M', the maximal $P700^+$ signal under light; F, the steady-state fluorescence signal; F_M', the maximal fluorescence signal under light) were monitored by the saturating pulse application at different irradiances, CO_2 and O_2 concentrations. The effective quantum yield of PSII [*Y(II)*] was calculated according to Genty *et al.* (1989). The effective quantum yield of PSI [*Y(I)*] and the non-photochemical yields of PSI caused by donor [*Y(ND)*] or acceptor [*Y(NA)*] side limitation were calculated as described in Klughammer and Schreiber (2008).

Four photosynthetic response curves (*A*/*PPFD* and A/C_i curves, under ambient and low [O_2]) were measured at 25 °C in daylong experiments. A/C_i curves were measured first, under a *PPFD* of 1000 µmol m^{-2} s^{-1} and imposing reference CO_2 concentrations of 20, 40, 60, 80, 100, 200, 300, 400, 500, 600, 800, 1000 µmol mol^{-1} and a minimum of 120 s between steps; *A*/*PPFD* curves were measured under reference [CO_2] of 420 µmol mol^{-1} imposing *PPFD*s of 1500, 1000, 200, 500, 150, 100, 75, 50, 30 µmol m^{-2} s^{-1} and a minimum of 180 s between steps. The order between ambient and low O_2 was inverted each day. Flow rate was 400 µmol s^{-1}; CO_2 diffusion through the gaskets was compensated by lengthening the tubing of the LI6400XT reference gas (Bellasio and Farquhar, 2019). Gas response curves were analysed using the protocol of Bellasio *et al.* (2016a). CO_2 concentration at the M carboxylation sites was calculated as $C_M = C_i - A/g_M$, where mesophyll conductance (g_M) was 1.5 for HL and 1.2 mol m^{-2} s^{-1} for LL derived by adjusting for S_m (Table 1) the data of Ubierna *et al.* (2017).

C_4 photosynthesis model

Biochemical models may include formulations describing a variety of processes (*e.g.*, electron transport), but, at any given time, only the formulation describing the process that is limiting photosynthesis in that circumstance will be representative (outputs are called 'actual' rates), while others are not [outputs are called 'potential' rates (Farquhar *et al.*, 1980)]. The mismatch between formulations can sometimes be useful, for instance, to estimate stomatal conductance in C_3 (Farquhar and Wong, 1984) and C_4 plants (Bellasio *et al.*, 2017), but typically it generates ambiguity in curve fitting [*e.g.*, fluorescence, reviewed in Bellasio *et al.* (2016b)] and difficulties in locating the cut-off points (Gu *et al.*, 2010). To avoid discontinuities, we merged enzyme limitations into a light-limited model by introducing a function describing the quenching of *Y(II)* depending on C_M, analogous to the classical *PPFD*-dependence of electron transport rate. This function depends on the familiar biochemical quantities V_{PMAX} and K_P, but we have not derived an explicit expression at this stage.

The model is organized to simulate two compartments representing M and BS cells (Figure 2): each harvests light to drive a distinct electron transport chain (Note S1, Figure S1). In both electron transport chains, the ratio between the rates of ATP and NADPH production is varied via adjustment of CEF (through the parameter f_{Cyc}), which may flow through PGR5/PGRL1 or the NAD(P)H dehydrogenase-like complex (NDH, adjusted through the parameter f_{NDH}). When f_{Cyc} is adjusted, the proportion of light absorbed by photosystems varies to maintain invariant the sum of light absorbed by the two [equations described in supporting information of Yin *et al.* (2004)]. This is of key importance when modelling energetics and CEF engagement under limiting light (Bellasio, 2019) because, otherwise, supplemental CEF would be driven by an increase in light absorbed [but *s* would be invariant, main text of Yin *et al.* (2004)]. The reducing power requirements for nitrogen reduction and for the water-water cycle are explicitly accounted for as a fraction of pseudo-cyclic electron flow, after Yin and Struik (2012), but we did not use the functionality in this study. A key innovation is that the rate of oxygen evolution in the BS is calculated from the actual rate of electron transport in both compartments, instead of being assumed to scale to assimilation through the parameter α as in all the models derived from Berry and Farquhar (1978).

ATP and NADPH drive the reactions of the carbon metabolism, described following Bellasio and Griffiths (2014c), McQualter *et al.* (2016), and Bellasio (2017). While the NADPH available in the BS is consumed by the RPP and the photorespiratory cycles, the ATP available in the M and any ATP surplus in the BS are consumed by the C_4 cycle, until all the ATP and NADPH available have been consumed. In this way, the partitioning between cycles and the apportioning of metabolic work between M and BS cells emerges directly from the rate

of ATP and NADPH produced by light reactions, instead of being assumed through the parameter x as in all the approaches following Berry and Farquhar (1978). Differently from Bellasio (2017), where all intermediate photosynthetic types were modelled, here C_4 photosynthesis is fully expressed, such that the glycine decarboxylase complex (GDC) and Rubisco are both fully compartmentalised to BS cells (Bellasio, 2017). However, C_4 subtypes can be changed seamlessly, forming a continuous biochemical space that can be explored by varying two parameters: f_{MDH}, representing the engagement of MDH in M cells and controlling the trajectory between the NADP-ME subtype and the NAD-ME subtype, and f_{PEPCK}, representing the capacity of PEPCK to consume ATP available in BS cells and representing the level of PEPCK expression relative to other carboxylases (we will explore these functionalities in dedicated studies). In the decarboxylation of malate, the co-products NADH and NADPH are assumed to be equivalent or interconvertible. This may be underpinned by an actual biochemical interconversion, mediated by the intercellular operation of the malate shuttle (Furbank, 2011), or simply by the capacity of malic enzyme (ME) to dock both cofactors, as suggested by early studies (Kanai and Edwards, 1973).

M and BS cells are connected by an exchange of metabolites (malate, MAL; phosphoenolpyruvate, PEP; pyruvate, PYR; aspartate, ASP; alanine, ALA; 3-phosphoglyceric acid, PGA; dihydroxyacetone phosphate, DHAP; and CO_2) which diffuse obeying mass balance constraints. Diffusion is non-limited, except that of CO_2, restrained by a finite conductance (g_{BS}) that allows higher CO_2 concentration in BS cells (C_{BS}) based on classical underpinnings (Berry and Farquhar, 1978). Glutamate and αKG do not diffuse directly between M and BS cells, but exchange amino-groups with ALA and PYR (Pick *et al.*, 2011, Mallmann *et al.*, 2014, Schlüter *et al.*, 2019). If reactions can proceed in opposite direction, they are assumed to proceed only in the direction with positive balance. Respiration is a shared process between M and BS cells. To avoid a futile cycle consisting of concurrent glycolysis and carbohydrate synthesis, respiration is assumed to be supplied by new assimilates (PGA) in line with Bellasio and Griffiths (2014c). The ATP and NADH produced during respiration are neglected, assumed to be consumed by basal metabolism. Any ATP and NADH residual imbalances produced during respiration in the light are absent, supported by the analysis of Buckley and Adams (2011) who proposed they would be dissipated by alternative oxidases. The final product of photosynthesis is a generic triose carbohydrate, whose destiny is not further followed by the model.

Details of the functions describing reaction rates and CO_2 and O_2 concentrations in M and BS compartments are provided in Supporting Note S2; reducing power poise is in Supporting Note S3 and metabolite flows in Note S4. Model sensitivity analysis is shown in Table S2.

Parameterisation

Parameters were either derived from measurements (in which case data was randomized and averaged for HL and LL plants), taken from dedicated studies, or assumed. Light penetration in the leaf was simulated through a separate optical model, freely downloadable from Supporting Information of Bellasio and Lundgren (2016). The number of layers of adaxial M cells was 289 for HL plants and 340 for LL plants; the number of layers of the vein was 458 for HL plants and 435 for LL plants; the number of layers of abaxial M cells was 253 for HL plants and 225 for LL plants; the fraction of interveinal distances occupied by the vein was 0.56 for HL plants and 0.532 for LL plants, all derived from anatomical measurements (Table 1). The absorbance of the adaxial M cells was set to equal that of M cells following the observation that BS extensions are absent in *S. viridis*; the absorbance of the vein relative to M cells $\left(\frac{k_{\mathrm{VB}}}{k_{\mathrm{MI}}}\right)$ was 1.65 for HL plants and 2.73 for LL plants, calculated by dividing the measured BS/M ratio of chlorophyll content per metre square of leaf, by the measured ratios of BS/M areas, 0.29 for HL and 0.24 for LL; reflectance was 0.067 for HL plants and 0.081 for LL plants (Table 1).

The combined model of light and dark reactions has 29 input quantities. Three define the environmental characteristics (*PPFD*, C_{M} and O_{M}), 17 define light reactions ($Y(II)_0$, s, $f_{\mathrm{Pseudocyc\ NR\ M}}$, $f_{\mathrm{Pseudocyc\ NR\ BS}}$, f_{Q}, h, $Y(I)_{\mathrm{LL}}$ $f_{\mathrm{NDH\ M}}$, $f_{\mathrm{NDH\ BS}}$, $f_{\mathrm{Cyc\ M}}$, $f_{\mathrm{Cyc\ BS}}$, α_{C}, $V_{0\,\mathrm{C}}$, θ_{C}, α_{V}, $V_{0\,\mathrm{V}}$, θ_{V}), six define dark reactions (f_{PH}, f_{PEPCK}, f_{RLIGHT}, f_{CS}, f_{MDH}), and three more (g_{BS}, $AB\ \frac{\mathrm{BS}}{\mathrm{M}}$, R_{LIGHT}) are not grouped. $AB\ \frac{\mathrm{BS}}{\mathrm{M}}$ was taken from the light penetration model described above, R_{LIGHT} and g_{BS} were derived from gas exchange and fluorescence measurements with the procedure described in (Bellasio *et al.*, 2016a) (Table S1). $Y(II)_0$ was derived by slightly increasing maximum values of $Y(II)_{\mathrm{LL}}$ so that Eqn S11 would return $Y(II)_{\mathrm{LL}}$ under ambient CO_2 concentration and zero *PPFD*. α_{C}, $V_{0\,\mathrm{C}}$, θ_{C}, α_{V}, $V_{0\,\mathrm{V}}$, θ_{V} were derived by fitting fluorescence data shown in Figure 3. s_0 is the theoretical maximum value of s when f_{Cyc} is zero was adjusted for modelled $s' = \frac{dGA_{Low}}{\frac{1}{3}Y(II)_{LOW}dI_{Inc}}$ to fit measured values of s′ (Table S1). The *Q*–cycle was assumed obligate making f_{Q}=1; $Y(I)_{\mathrm{LL}}$ was assumed 1 after Yin and Struik (2012). The behaviour of $f_{\mathrm{Pseudocyc\ NR\ BS}}$ and $f_{\mathrm{Pseudocyc\ NR\ M}}$ in response to CO_2 and *PPFD* is not well known,

therefore we assumed a low value for simplicity. The stoichiometry of the ATP synthase was set at h=4.67 H^+ per ATP after structural evidence (Vollmar *et al.*, 2009, Hahn *et al.*, 2018). The operation of NDH is essential for C_4 photosynthesis, but estimates for the electron flow through the complex are unknown, and difficult to imagine. Here f_{NDH} was set to 0.4 in M cells and 0.7 in BS cells following the observation that NDH- and PGR5-mediated electron flows are both operating in C_4 plants (Takabayashi et al. 2005) while keeping in mind that the relative ratio of NDH to PSI was higher in BS cells than in M cells (Ermakova *et al.*, 2021b). $f_{Cyc\ M}$ and $f_{Cyc\ BS}$ were fitted to maximise A at each light intensity subject to the constraint that the activity of PPDK in BS cells is zero; fitted values are shown in Figure S3. f_{RLIGHT} and f_{CS} were set 0.5 after von Caemmerer (2000) and Bellasio (2017). f_{PEPCK} was set to zero to match immunoblotting (Figure 5). f_{PH} is irrelevant under the previous assumption. f_{MDH} sets the transition between NAD–ME and NADP–ME subtypes and was assumed to be 1 (Gutierrez *et al.*, 1974, John *et al.*, 2014).

Statistical analysis

The relationship between mean values for HL and LL plants was tested using a two-tailed, heteroscedastic Student's t-test at $P < 0.05$ (Microsoft Excel® 2016). Error propagation in the model was not analysed.

Results

Leaf anatomy and chlorophyll

In HL plants, BS chloroplasts were uniformly distributed inside the cells (Figure 1). In LL plants, BS chloroplasts had clear centrifugal position whilst M chloroplasts were specifically arranged along the cell walls, particularly in adaxial M cells. This was captured by a higher apparent absorbance of M cells of HL plants (Table 1). Increased number of chloroplasts in adaxial BS cells compared to abaxial ones was more prominent in LL plants. In line with the higher chlorophyll content in the BS of LL plants relative to the M, LL vascular bundles showed increased apparent absorbance (Table 1). LL leaves had 15 % lower M thickness as well as 10 % lower interveinal distance compared to HL plants. The BS surface area per leaf area (S_b) was 13 % lower, and the M surface area exposed to the intercellular airspace (S_m) decreased by 35 %, in LL plants compared in HL plants.

Gas-exchange and yield of photosystems

When the light–response was measured at 420 µmol mol^{-1} CO_2 and 21 % O_2, no difference was significant between HL and LL plants in CO_2 assimilation rate (*A*) or effective quantum yields of PSII [*Y(II)*] and PSI [*Y(I)*] (Figure 3). Yields of non-photochemical losses in PSI due to the donor [*Y(ND)*] and acceptor [*Y(NA)*] side limitations did not differ between the two growth regimes (Figure 3g). At 2 % O_2, no differences in light responses between HL and LL plants were detected (Figure 4).

CO_2 response curves were measured at a *PPFD* of 1000 µmol m^{-2} s^{-1} either at 21 % or 2 % O_2. No differences in CO_2 assimilation, *Y(II)*, *Y(I)*, *Y(ND)* or *Y(NA)* were significant between HL and LL plants independently of O_2 level (Figure 3, Figure 4). Both HL and LL plants showed decreased *Y(II)* and increased *Y(ND)* at low $C_{M,}$ likely, representing an induction of non–photochemical quenching in the PSII antennae in response to the acidification of the thylakoid lumen. The latter is induced by the downregulation of ATP synthase activity in response to the reduced ATP consumption by the RPP cycle (Kanazawa and Kramer, 2002). Interestingly, *Y(NA)* at low C_M was higher when measured at 2 % O_2 (Figure 3h, Figure 4h), pointing to a contribution of O_2 to oxidating PSI via photorespiration and/or O_2 photoreduction (Sagun *et al.*, 2021).

To aid interpretation of light and CO_2 response curves, we fitted empirical and mechanistic models after Bellasio *et al.* (2016a). Fitted parameters in Table S1 show that, under ambient O_2, the main differences were dependent on a decrease of respiration in the light (R_{LIGHT}), light compensation point (*LCP*), CO_2 compensation point (Γ) and BS conductance to CO_2 diffusion (g_{BS}) in LL plants. Curiously, O_2 sensitivity of R_{LIGHT}, quantum yield [$Y(CO_2)_{LL}$] and carboxylation efficiency was opposite between HL and LL plants. The decrease in photosynthetic efficiency in LL plants under low [O_2] supports a more important role of O_2 in photoprotection of LL plants (Sagun *et al.*, 2021). A link between electron transport and R_{LIGHT} is known to exist (Buckley and Adams, 2011), but it is not characterised in C_4 plants. Of the fitted quantities, only R_{LIGHT} and g_{BS} were retained for model parameterisation, detailed above.

Modelling of light distribution, light reactions and dark metabolism

Using measured anatomical characteristics, BS/M chlorophyll ratio and leaf absorptance (Table 1), we modelled light penetration through the leaf profile according to Bellasio and Lundgren (2016). Absorbed light in the BS relative to M was higher in HL plants ($AB\ \frac{\mathrm{BS}}{\mathrm{M}}$ was 0.414 for HL and 0.343 for LL, Table 1). Next, to gain comprehensive understanding of the photosynthetic metabolism, we used these values, *Y(II)*, g_{BS} and R_{LIGHT} derived from the

concurrent gas–exchange and chlorophyll fluorescence measurements (Table S1), to parameterise a purposely derived model of light reactions and dark metabolism, while the fraction of electron flow through PSI following CEF in M and BS ($f_{\mathrm{Cyc\,M}}$ and $f_{\mathrm{Cyc\,BS}}$, respectively) were fitted to maximise assimilation, constrained to maintain PPDK and PEPCK activity in BS cells at zero to match immunoblotting (Figure 5).

Initially, we replicated *in silico* the leaf gas–exchange measurements under ambient O_2 level (Figure 3). For both light and CO_2 response curves, the trends of CO_2 assimilation and *Y(II)* were well captured by the model. For assimilation, R^2 was 0.98 and 0.97 in light curves or 0.95 and 0.81 in A/C_i curves of HL and LL plants, respectively. For *Y(II)*, R^2 was 0.86 and 0.96 in light curves or 0.91 and 0.76 in A/C_i curves of HL and LL plants, respectively. In the light response curves, the model captured a hyperbolic decrease of the measured *Y(I)* at high irradiance (Figure 3e) but not an initial dip at low irradiance. However, the modelled *Y(I)* was similar to the trend of 1 - *Y(ND)*, perhaps only capturing *Y(I)* available due to the electron input from PSII but not accounting for the loss of *Y(I)* due to the unavailability of acceptors, that is, *Y(NA)*. In CO_2 response curves, the hyperbolic increase of *Y(I)* was captured, but *Y(I)* was slightly underestimated for C_M greater than 20 μmol mol^{-1}. Predicted *Y(I)* did not differ between HL and LL plants.

Next, we carried out a simulation of photosynthetic biochemistry using the specific parameterisation of growth light regimes (Table 2). LL plants had a 60 % downregulation of assimilatory metabolism due to the lower energy availability (Table 3, to aid comparison between light regimes we also expressed fluxes in multiples of gross assimilation). Because of the lower NADPH availability, LL plants exported a higher fraction of the total PGA produced to the M for reduction than HL plants (42% and 35%, respectively, Table 3). Rubisco carboxylation (V_C) and PEP carboxylation rate (V_P, which corresponds to the rate of malate export to BS cells and the backflux of pyruvate) had lower activity in LL plants. The decrease in V_P caused a 25 % decrease in CO_2 concentration in the BS that was reflected by a higher ratio of Rubisco oxygenation relative to carboxylation (V_O/V_C, 4.9 % in HL plants and 5.4 % in LL plants, Table 3). However, there was a general increase in PSII efficiency in LL plants which overweighed the effect on V_O/V_C. As a result, in LL plants the average quantum yield increased 38 % on absorbed light basis (from 0.04 to 0.055 CO_2/quanta), and as much as 43 % on incident light basis (from 0.031 to 0.044 CO_2/quanta) as compared to HL plants. LL plants gained more on incident light basis because of their higher leaf absorbance (captured in the measurements by s', Table S1, and in the model inputs by s_0, Table 2).

Discussion

S. viridis is a wild ancestor of *S. italica* (foxtail millet), a grain crop widely grown in China and India. It has gained favour for studying C_4 photosynthesis because it has a rapid life cycle, small stature, sequenced genome and available genetic transformation method (Brutnell *et al.*, 2010, Ermakova *et al.*, 2021c). Since C_4 photosynthesis has evolved independently at least 70 times (Sage, 2017), diverse biochemical arrangements are possible in C_4 plants, and characterising different approaches of shade acclimation is a prerequisite for identifying best targets for improving crop performance. While anatomical responses of C_4 plants to shading are relatively conserved (Ward and Woolhouse, 1986, Pengelly *et al.*, 2010), biochemical strategies appear to be diverse.

We recently showed that *S. viridis* grown at limiting irradiance deployed a suite of protein level adjustments providing BS thylakoids with increased capacity for light harvesting and electron transport and pointing to an increased ATP demand in the BS (Ermakova *et al.*, 2021b). Here, we were interested in resolving whether the observed rearrangements were triggered by an increased ATP consumption from dark reactions or by a lower rate of production, perhaps, due to anatomical modifications. Whilst acclimation to LL generally entails a downregulation of photosynthetic potential, here gas exchange measurements showed that HL and LL plants reached strikingly similar rates of assimilation when measured at the same light or CO_2 levels. This intriguing invariance, which we repeatedly measured in plants from different growth batches, and was previously observed in the same ecotype independently (Henry *et al.*, 2019), may be a particular feature of *S. viridis*. Detailed analysis of the response curves through model fitting (Table S1) revealed some contrasting acclimation strategies: LL plants had lower carboxylation efficiency and lower $Y(II)_{LL}$, but also lower respiration, than HL plants. We then characterised the leaf anatomy and found a reduction in BS size and in BS surface area per leaf area (S_b) in LL plants. Our interpretation is that these anatomical changes concurred to the reduction of g_{BS} (von Caemmerer *et al.*, 2008), here estimated by fitting of gas exchange and fluorescence data obtained under ambient and low [O_2]. The reduction of g_{BS} at low light is consistent with previous results obtained through different proxies including anatomy, isotopic discrimination, combined gas exchange and chlorophyll fluorescence (Pengelly *et al.*, 2010, Ubierna *et al.*, 2013). Interestingly, g_{BS} was shown to decrease both in plants grown under low light (Bellasio and Griffiths, 2014b) and in plants grown under high light subsequently transferred to low light, as it occurs in crop canopies where older leaves are shaded by new growth (Bellasio and Griffiths, 2014a).

The decrease in g_{BS} ameliorates the efficiency of C_4 photosynthesis. By hindering CO_2 leakage, it counters the decrease in CO_2 concentration in the BS and the increase of photorespiration occurring under low light (Kromdijk *et al.*, 2014). However, the associated reduction in BS size (Table 1) has the undesirable consequence of decreasing the light harvesting in BS cells, limiting ATP generation and decreasing the operational plasticity under changing light conditions (Bellasio and Lundgren, 2016). LL plants deployed a concerted suite of responses to counter potential ATP starvation in the BS. Firstly, while in HL plants M chloroplasts were dispersed, in LL plants the arrangement of M chloroplasts along the cell walls (Figure 1), similar to that observed in *Saccharum officinarum* grown under low light (Sales *et al.*, 2018), created optical gaps, resulting in lower apparent absorbance of the M and increasing the amount of light filtering through to BS cells (Table 1), a phenomenon known as 'sieve effect' (Terashima *et al.*, 2009). Chloroplast arrangements differ depending on species, light quality and intensity. For instance, under midday illumination *Eleusine coracana* was shown to aggregate M chloroplasts around the BS; *Zea mays* showed a dispersed arrangement, similar to what we observed in *S. viridis*; *Sorghum bicolor* created characteristic optical corridors spanning the whole leaf thickness, presumably aiding photoprotection, observed also in *Z. mays* but only under non–physiological irradiance (3,000–4,000 μmol m^{-2} s^{-1}) (Yamada *et al.*, 2009, Maai *et al.*, 2020a, Maai *et al.*, 2020b). Secondly, in LL leaves the BS had higher chlorophyll content (Table 1) and increased abundance of light-harvesting complexes (LHC) I and II compared to HL plants (Ermakova *et al.*, 2021b). Consistently, LL leaves had higher absorptance (Table 1), and fitting of combined gas exchange and fluorescence data captured a higher s′, the parameter representing effective leaf level light interception lumped to the yield of ATP generation (Table S1). Thirdly, the potential of BS thylakoid membranes for ATP production increased due to the upregulation of PSI, Cytochrome b_6f, ATP synthase and NDH (Ermakova *et al.*, 2021b). The latter has been shown to be beneficial for C_4 photosynthesis in reverse genetics studies (Ishikawa *et al.*, 2016, Peterson *et al.*, 2016) and found to correlate with the ATP requirements of cell types in C_4 plants (Takabayashi *et al.*, 2005).

Next, we were interested in resolving to what extent the observed reorganisations of light harvesting and electron transport processes in LL plants was effective in countering the limitations to ATP generation caused by a smaller BS, and what modifications to the metabolism of BS and M were required to maintain invariant levels of assimilation (Figure 3). We developed a model encompassing explicit anatomy and separate electron transport chains in the BS and M, parameterised specifically for HL and LL plants. We found that the increased chlorophyll concentration was not sufficient to counter the effect of smaller BS cells size and,

overall, LL plants absorbed 40 % less light in BS cells relative to total (from 23 % under HL to 14 % under LL, Table 3). However, the higher proportion of CEF (f_{Cyc}) in BS of LL plants (Table 3, Figure S3) could partially compensate for the decrease in light absorption, so that the predicted ATP production rate, relative to total, only decreased by about 5 % (from 45 % in the BS of HL plants to 42 % in the BS of LL plants, Table 3). The predicted changes in f_{Cyc} – an emerging property of the fitted model mainly resulting from the reduction in BS size – are in line with the increased content of NDH detected in LL BS cells (Ermakova *et al.*, 2021b), again pointing to the key role of NDH in ATP production in BS cells. Hence, we demonstrated that: first, the upregulation of CEF (f_{Cyc}) is effective in mitigating decreased light interception in BS cells, and, second, that decreasing light interception in BS cells is a sufficient condition to require an increase of f_{Cyc} (Table 3, Figure S3). To our knowledge this functional dependence was not demonstrated before, uncovering another important link between biochemical properties and structural characteristics of C_4 leaves.

The NADPH production rate in BS cells relative to total was predicted to decrease 97 % in LL plants (from 11 % under HL to 0.3 % under LL), driven both by the decrease in BS size and increase in f_{Cyc}. This led to a 13 % decrease in the rate of PGA reduction in BS cells relative to total (from 66 % under HL to 59 % under LL), and a consequent relative increase of triose fluxes between M and BS cells in LL plants (Table 3). By means of LEF, PSII activity in BS cells not only supplies NADPH production, but also replenishes CEF electrons leaking to various electron sinks downstream of PSI (explicitly accounted for in the model as pseudocyclic electron flow, but not varied in this study). In this model output, LEF in the BS was predicted to be 21 µmol m^{-2} s^{-1} (14 % of the total leaf rate for HL plants), and 5.59 µmol m^{-2} s^{-1} (9 % of the total leaf rate for LL plants, Table 3). The actual PSII activity in the BS thylakoid membranes measured by Ermakova *et al.* (2021b) matched the value predicted for LL plants (it was circa 7 % of the leaf rate), but in HL plants it was a half of the LL value, much lower than the model prediction. This suggests that the predicted value of J_2 in the BS of HL plants cannot be supplied *in vivo* by electrons coming from water oxidation, but must be obtained via oxidation of NADPH, derived from malate imported from the M, through the NDH. This idea is supported by experimental observations. When supplied with malate, isolated BS strands of *Z. mays* retained PSI activity even in the presence of PSII inhibitor. Further, the BS of *S. bicolor* maintained CO_2 fixation under far–red illumination, which is unable to excite PSII (Osmond, 1974, Ivanov *et al.*, 2005).

Theory shows that, under changing irradiance, flexibility in the apportioning of PGA reduction between BS and M cells can regulate the BS demand of NADPH, and the engagement

of PEPCK and PPDK can attune the BS demand of ATP (Furbank, 2011, Bellasio and Griffiths, 2014c). Because PEPCK consumes ATP generated in the M and is tightly regulated by ATP availability, the expression of PEPCK in NADP–ME plants was predicted to increase light harvesting plasticity, *i.e.,* the capacity to efficiently harvest light in a broad range of intensity and spectral quality (Bellasio and Griffiths, 2014c). Further, the activity of PPDK in the BS could compensate for a lack of PEPCK, making PEPCK engagement necessary when the activity of PPDK in the BS was reduced, and *vice versa* (Bellasio, 2017). Indirect evidence supports these predictions. It was shown that low light acclimated NADP–ME plants, like *Z. mays* and *S. officinarum,* increased the total rate of PEPCK activity (Sales *et al.*, 2018) or the activity of PEPCK relative to PEPC (Sharwood *et al.*, 2014, Sonawane *et al.*, 2018), and increased the pool of inactive PEPCK (data made available by courtesy of B.V. Sonawane, personal communication), presumably available to be activated by changing light conditions (Bailey *et al.*, 2007).

Uniquely, *S. viridis* did not express PEPCK neither under HL nor under LL (Figure 5). Nor we found detectable levels of PPDK in the BS (Figure 5), in line with previous reports (John *et al.*, 2014, Schlüter and Weber, 2020). Although *Z. mays* grown under low light overexpressed LHCII subunits and PsbD in BS cells (Drozak and Romanowska, 2006), it did not show increased oxygen activity or changes in supramolecular organisation of PSII (Romanowska *et al.*, 2006, Rogowski *et al.*, 2019). In contrast, *S. viridis* had a striking plasticity in acclimating light reactions, probably sufficient to avoid the necessity to regulate PEPCK and PPDK expression (Figure 5). Importantly, and differently from the nine species (four NADP–ME including *Z. mays* and *S. bicolor*, two NAD–ME, two PEPCK) studied by Sonawane *et al.* (2018), acclimation of light reactions in *S. viridis* did not compromise quantum yield (Table S1). Therefore, the outstanding capacity of *S. viridis* to rearrange light reactions under low light is a highly efficient acclimation strategy setting *S. viridis* aside from other NADP–ME plants and representing a so far overlooked innovation in C_4 evolutionary history.

Conclusion

Using a purposely developed model, parametrised with original anatomical, biochemical, and gas exchange data, we analytically and mechanistically solved the causality link between anatomy and biochemistry. The optical cross section determined the absorption of light in the BS and the M, the rate of electron transport, the engagement of CEF and LEF, the rate of ATP and NADPH generation, and ultimately the apportioning of carbon metabolism between M and BS cells. To counter ATP starvation, *S. viridis* adjusted electron transport processes, boosting

cycling electron flow in the BS. Although quantifying the impact in field conditions will require additional experiments, the striking capacity of *S. viridis* to acclimate light reactions is perhaps the most efficient shade tolerance strategy, potentially leading to novel possibilities for crop improvement.

Availability

Data and the model, coded in **R** and Microsoft® Excel®, are made freely available in the Supporting Information and on GitHub at the link [to be provided during copyediting].

Author contributions

ME and CB conceived the project. CB developed the model and ran simulation. CB and ME performed experiments, analysed the data and wrote the article. Authors declare no conflict of interest.

Acknowledgements

We are deeply grateful to Graham Douglas Farquhar for hospitality and to Suan Chin Wong, Dean Price and Susanne von Caemmerer for equipment. We thank Russell Woodford for coding in R, Balasaheb Vitthal Sonawane for data and discussion, Riya Kuruvilla and Tegan Norley for technical assistance. We thank Florence Danila, Joanne Lee and Centre for Advanced Microscopy at the Australian National University for preparing and imaging leaf cross-sections. We thank the Australian Plant Phenomics Facility supported under the National Collaborative Research Infrastructure Strategy of the Australian Government. CB was funded by H2020 Marie Skłodowska-Curie individual fellowship (DILIPHO, ID: 702755). ME was supported by the Australian Research Council Centre of Excellence for Translational Photosynthesis (CE140100015).

Table 1. Anatomical and biochemical characteristics of leaves, mesophyll (M) and bundle sheath (BS) cells of *S. viridis* grown at high light (1000 µmol m^{-2} s^{-1}, HL) or low light (300 µmol m^{-2} s^{-1}, LL). Mean values are shown ± SE, n = 20 (except for chlorophyll and leaf absorptance n = 3, apparent absorbance n = 6). Asterisks indicate statistically significant difference between two light regimes ($P < 0.05$).

Characteristic	HL	LL
Height at vein (µm)	238 ±12.2	205 ±8.5*
Interveinal distance (µm)	181.5 ±4.8	165 ±4.8*
Abaxial Mesophyll Height (µm)	60.2 ±3.3	46.0 ±2.5*
Adaxial Mesophyll Height (µm)	68.8 ±3.2	69.7 ±3.7
Bundle sheath area (µm^2)	9604 ±1101	6719 ±763*
Vein width (µm)	98.1 ±6.5	89.1 ±5.11
Chlorophyll (*a*+*b*) in the M (mmol m^{-2} leaf)	0.27 ±0.01	0.38 ±0.01*
Chlorophyll (*a*+*b*) in the BS (mmol m^{-2} leaf)	0.13 ±0.01	0.25 ±0.04*
Mesophyll surface area exposed to intercellular airspace, S_m (m^2 m^{-2})	14.13 ±0.4	9.12 ±0.5*
Bundle sheath cells surface area per unit of leaf area, S_b (m^2 m^{-2})	2.21 ±0.06	1.92 ±0.04*
Leaf absorptance	0.789 ±0.02	0.855 ±0.04*
Mesophyll apparent absorbance (from micrograph luminance)	0.168±0.01	0.117±0.01*
Vascular bundle apparent absorbance (from micrograph luminance)	0.288±0.01	0.344±0.02*

Table 2. Model inputs and sources.

Symbol	**Description**	**unit**	**HL**	**LL**	**Source**
PPFD or I_{inc}	Photosynthetic photon flux density	µmol m^{-2} s^{-1}	1000 or variable	1000 or variable	equal to measurements
C_M	CO_2 concentration in M cells	µmol mol^{-1}	variable or 400	variable or 400	-
O_M	O_2 concentration in M cells	µmol mol^{-1}	210000	210000	equal to ambient
g_{BS}	Bundle sheath conductance to CO_2 diffusion	mmol m^{-2} s^{-1}	0.0018	0.0012	Gas exchange curve fitting
γ^*	Half the reciprocal Rubisco specificity		0.00031	0.00031	(Boyd *et al.*, 2015)
R_{LIGHT}	Respiration in the light	µmol m^{-2} s^{-1}	1.93	1.18	Gas exchange curve fitting
Chl BS/M	Chlorophyll (*a*+*b*) in the BS relative to M	$\left(\frac{\text{mmol m}^{-2}\ \text{Leaf}}{\text{mmol m}^{-2}\ \text{Leaf}}\right)$	0.48	0.66	Spectroscopic measurements (Table 1)
AB BS/M	Fraction of light absorption in BS cells relative to M cells		0.414	0.343	Light penetration and anatomy model (Bellasio and Lundgren, 2016)
$Y(II)_0$	Yield of PSII extrapolated under zero *PPFD* and infinite C_M		0.76	0.73	1.04 × $Y(II)_{LL}$
s_0	lumped energy conversion coefficient when f_{Cyc}=0 (Yin *et al.*, 2009), similar to αβ in other notations	e$^-$/quanta	0.440	0.463	fitted for $\frac{d\,GA_{LOW}}{\frac{1}{3}Y(II)_{LOW}\,dI_{Inc}} = s'$
$f_{PSEUDO\ NR\ M}$	Fraction of J_1 following used by nitrate reduction in M cells		0.01		Assumed low for simplicity
$f_{PSEUDO\ NR\ BS}$	Fraction of J_1 following used by nitrate reduction in BS cells		0.01		Assumed low for simplicity
f_Q	Fraction of J_1 going through the Q-cycle		1	1	(Yin and Struik, 2012)
h	Stoichiometry of ATP synthase: protons required to synthesize ATP	h$^+$/ATP	4.67	4.67	(Vollmar *et al.*, 2009, Hahn *et al.*, 2018)
$Y(I)_{LL}$	Yield of PSI extrapolated under zero *PPFD*		1	1	(Yin and Struik, 2012)
$f_{NDH\ M}$	Fraction of CEF through the NDH complex in the M		0.4	0.4	see *Parameterisation*
$f_{NDH\ BS}$	Fraction of CEF through NDH in BS cells		0.7	0.7	see *Parameterisation*
$f_{Cyc\ M}$	Fraction of J_1 following CEF in M cells		fitted to max *A*	fitted to max *A*	
$f_{Cyc\ BS}$	Fraction of J_1 following CEF in BS cells		fitted to max *A*	fitted to max *A*	
α_C	Slope of the non–rectangular hyperbola used to model $f(CO_2)$		0.15	0.15	fitted to fluorescence
V_{0C}	y-intercept of the non–rectangular hyperbola used to model $f(CO_2)$		1	1	assumed 1 for simplicity
θ_C	Curvature of the non–rectangular hyperbola used to model $f(CO_2)$		0.3	0.3	fitted to fluorescence
α_V	Slope of the non–rectangular hyperbola used to model *f(PPFD)*		0.0004	0.0004	fitted to fluorescence
V_{0V}	y-intercept of the non–rectangular hyperbola used to model *f(PPFD)*		1	1	assumed 1 for simplicity
θ_V	Curvature of the non–rectangular hyperbola used to model *f(PPFD)*		0.8	0.8	fitted to fluorescence
f_{PH}	Fraction of PEP produced by PEPCK that is hydrolysed		-	-	irrelevant because f_{PEPCK}=0
f_{PEPCK}	Fraction of the activity of PECK relative to the maximum (that is the fraction of $J_{ATP\ BS}$ not used by the RPP and PCO cycle)		0	0	Immunoblotting (Fig. 3)
f_{RLIGHT}	fraction of respiration in the light in BS cells relative to leaf-level		0.5	0.5	(von Caemmerer, 2000)
f_{CS}	Fraction of carbohydrate synthesis in BS cells		0.5	0.5	(Bellasio, 2017)
$f_{MDH\ M}$	Fraction of M activity of MDH, relative to its maximum, defines the transition between NAD-ME and NADP-ME		1	1	(John *et al.*, 2014)

Table 3. Output of the combined light reaction and biochemical model of C_4 photosynthesis. The output shown is calculated at the growth *PPFD* (1000 for HL or 300 µmol m^{-2} s^{-1} for LL), and expressed, except for f_{Cyc} and Φ (dimensionless) or *C* (µmol mol^{-1}), in µmol m^{-2} s^{-1} and in brackets as a fraction of gross assimilation at the growth light (30.97 for HL and 13.24 µmol m^{-2} s^{-1} for LL plants).

		HL		LL	
Symbol	**Description**	**M**	**BS**	**M**	**BS**
f_{Cyc}	Fraction of electron flow through PSI (J_1) following CEF	0.01	0.783	0.08	0.866
C	CO_2 concentration	400	4100	400	3100
I_{Inc}	Incident light (*PPFD*)	707 (23.5)	293 (9.71)	223 (17.7)	77 (6.08)
I_2	Light absorbed by PSII	310 (10.0)	50 (1.63)	100 (7.54)	9.5 (0.718)
I_1	Light absorbed by PSI	238 (7.68)	176 (5.69)	79.1 (5.97)	51.9 (3.92)
J_2	Electron flow through PSII	151 (4.88)	25 (0.794)	63.8 (4.82)	6.07 (0.458)
J_1	Electron flow through PSI	153(4.92)	113 (3.65)	69.2 (5.22)	45.4 (3.43)
J_{NADPH}	NADPH production rate (half the electron flow to NADPH)	58.8 (1.90)	7.09 (0.229)	27.4 (2.07)	0.948 (0.07)
J_{ATP}	ATP production rate	97.9 (3.16)	80.2 (2.59)	44.2 (3.34)	32.5 (2.46)
V_P	PEP carboxylation rate. Because in this study f_{MDHM}=1, V_P corresponds to the rate of malate flux to the BS, the rate of pyruvate flux to the M, the PPDK reaction rate in the M (PPDK reaction rate in the BS is fitted to be zero in this study) and the malic enzyme reaction rate	36.7 (1.18)	0	15.9 (1.20)	0
L	Leakage rate of CO_2 out of the BS	6.64 (0.214)		3.21 (0.242)	
Φ	Leakiness: CO_2 leakage rate out of the BS relative to V_P	0.18		0.20	
V_C	Rubisco rate of carboxylation	0	31.7 (1.02)	0	13.6 (1.03)
V_O	Rubisco rate of oxygenation	0	1.54 (0.0496)	0	0.735 (0.0555)
PR	Rate of PGA reduction	22.2 (0.716)	43.0 (1.39)	11.5 (0.868)	16.4 (1.24)
$DHAP_{RPP}$	Rate of DHAP entering the conversion phase of the RPP cycle	0	55.5 (1.79)	0	23.9 (1.81)
RuP_{Phosph}	Rate of RuP phosphorylation	0	33.3 (1.07)	0	14.3 (1.08)
CS	Rate of carbohydrate synthesis	4.85 (0.156)	4.85 (0.156)	2.01 (0.152)	2.01 (0.152)
R_{Light}	Rate of respiration in the light	0.95 (0.031)	0.95 (0.031)	0.590 (0.047)	0.590 (0.046)
PGA flux	Flux of PGA	22.5 (0.726)	-22.5 (-0.726)	11.7 (0.882)	-11.7 (-0.882)
DHAP flux	Flux of DHAP	-17.3 (-0.559)	17.3 (0.559)	-9.48 (-0.716)	9.48 (0.716)

Figure 1. Light microscopy images of the leaf cross-sections used for anatomical measurements from *S. viridis* grown under high light (1000 µmol m^{-2} s^{-1}, HL) or low light (300 µmol m^{-2} s^{-1}, LL).

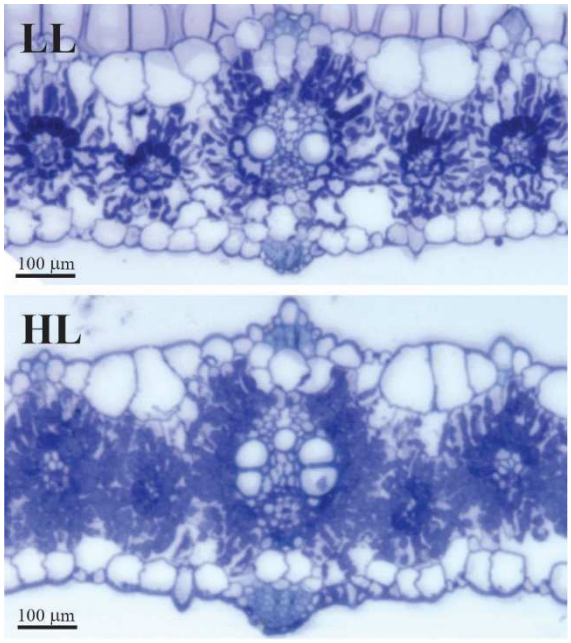

Figure 2. Schematic of the processes included in the model. Metabolites are in black; fluxes are schematised by black arrows and pink symbols which directly link to equations reported in Supporting Notes; key processes are briefly described in bright green. The leaf is divided into M and BS compartments. Incident *PPFD* (I_{inc}) may reach M ($I_{Inc\ M}$) or BS cells ($I_{Inc\ BS}$) depending on anatomical characteristics and size of the light-harvesting machinery. A fraction I is absorbed by PSI or PSII (I_1 or I_2, respectively). Light reactions (for more details see Figure S1) result in the production of NADPH and ATP, which are consumed by carbon metabolism encompassing C_4 and C_3 activity. The C_4 cycle reactions appear in the centre of the M and BS compartments. CO_2 is initially hydrated to bicarbonate (the point of entry is highlighted in yellow) and fixed by PEP carboxylase (PEPC) at the rate V_P to form oxaloacetate (OAA). This may be reduced to malate (MAL) or to aspartate (ASP) through transamination (T), *i.e.*, the exchange of amino-groups with glutamate (GLU). MAL and ASP both diffuse to BS cells; MAL is decarboxylated with the concurrent reduction of NADP by malic enzyme (ME) while ASP is deaminated to OAA (the exchange of amino-groups with alpha-ketoglutarate (αKG) is implied) and may be decarboxylated by PEP carboxykinase (PEPCK) or by malic enzyme (ME). The regeneration of PEP is shared between M and BS cells depending on energy availability. The C_3 metabolism appears at the bottom, partitioned between M and BS compartments. Rubisco carboxylation and oxygenation reactions (V_C and V_O) consume RuBP and produce PGA and PGLA and are fully compartmentalised to BS cells. PGLA is recycled through the photorespiration cycle eventually regenerating PGA. This is consumed by respiration (R_{LIGHT}), assumed to be entirely supplied by newly

assimilated PGA, and is reduced (*PR*) to triose phosphate (DHAP), which is a substrate of carbohydrate synthesis (CS). The final product of photosynthesis is a generic triose carbohydrate (highlighted in yellow). The majority of DHAP enters the sugar conversion phase of the reductive pentose phosphate (RPP) cycle, exclusive to the BS. Metabolites for which fluxes are calculated are listed in the middle, and assumed to be positive when occurring in the ordinary direction indicated by arrows. The Excel workbook provided renders outputs according to this scheme.

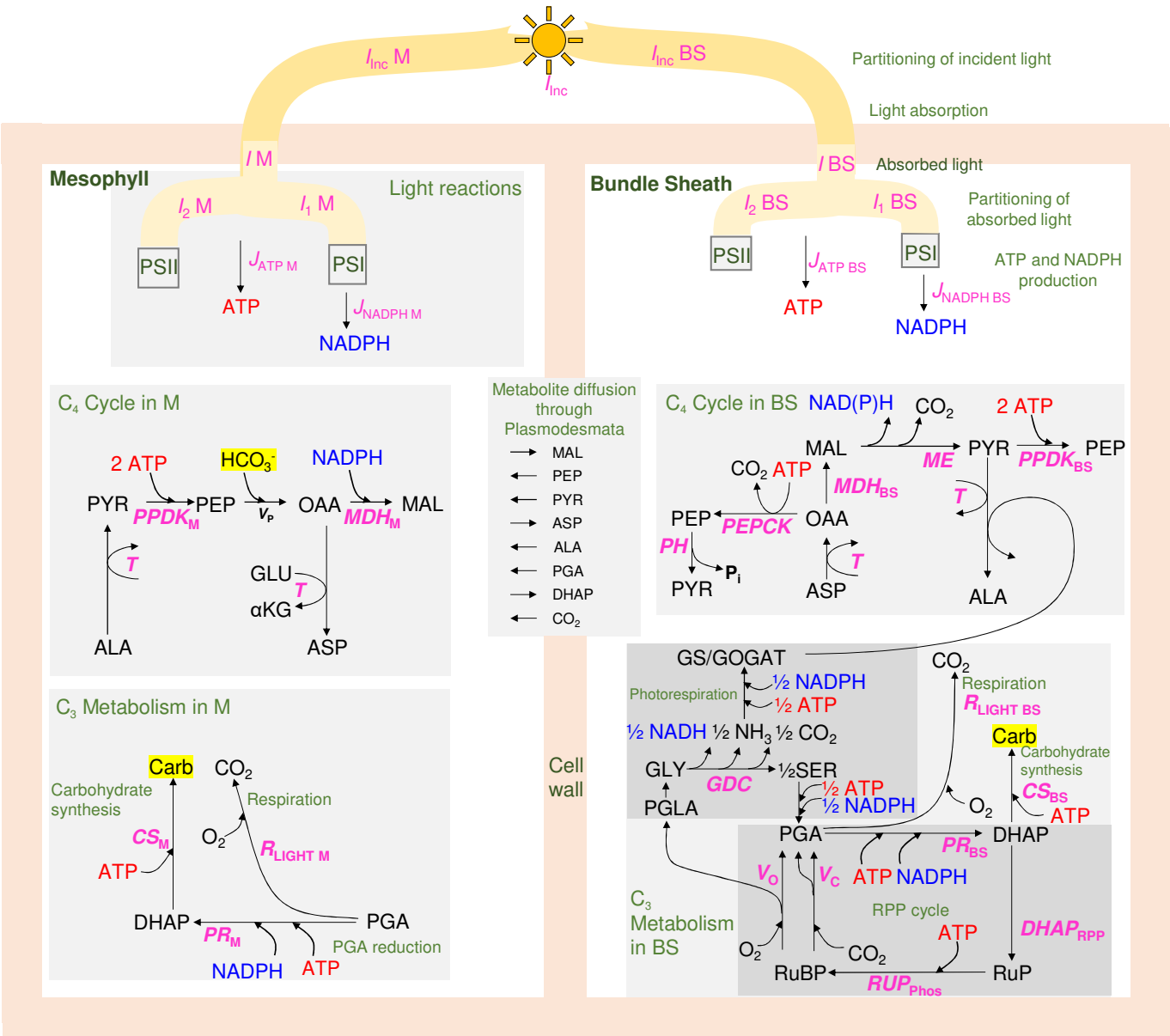

Figure 3. Measured and modelled gas exchange and photosystems yield under ambient O_2 level. Symbols show response curves of CO_2 assimilation (**a**, **b**), quantum yield of Photosystem II (**c**, **d**), quantum yield of Photosystem I (**e**, **f**), Photosystem I donor [*Y(ND)*] and acceptor side [*Y(NA)*] limitations (**g**, **h**) obtained for *S. viridis* grown at high light (HL, solid circles) and low light (LL, empty circles). Light curves measured under a reference [CO_2] of 420 µmol mol^{-1} are shown in left panels, and CO_2 response curves obtained under constant irradiance of 1000 µmol m^{-2} s^{-1} are shown in right panels. Mean ± SE, n = 3 biological replicates. C_M, CO_2 concentration in M cells. Corresponding curves obtained by switching the background gas to low O_2 are shown in Figure 4. Lines show modelled responses obtained through a combined biochemical model of light reactions and carbon metabolism of C_4 photosynthesis. Model parameters are listed in Table 2.

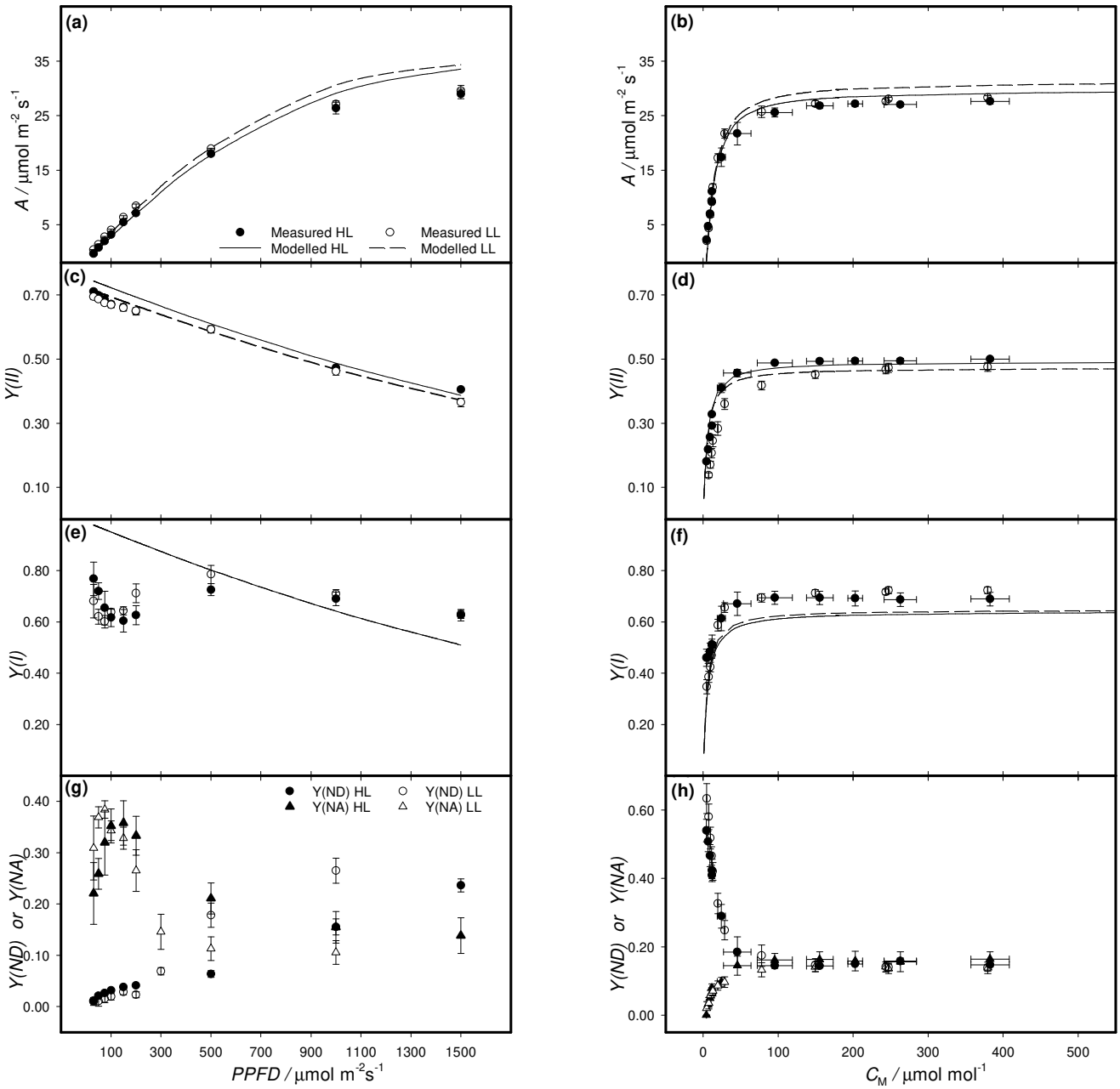

Figure 4. Measured gas exchange and photosystems yield at 2 % O_2. Light curves measured under a reference [CO_2] of 420 µmol mol^{-1} are shown in left panels, CO_2 response curves obtained under constant irradiance of 1000 µmol m^{-2} s^{-1} are shown in right panels. Symbols show response curves of CO_2 assimilation (**a**, **b**), quantum yield of Photosystem II (**c**, **d**), quantum yield of Photosystem I (**e**, **f**), Photosystem I donor side [*Y(ND)*] and acceptor side [*Y(NA)*] limitations (**g**, **h**) obtained for *S. viridis* grown at high light (HL, solid circles) and low light (LL, empty circles). Mean ± SE, n = 3 biological replicates. C_M, CO_2 concentration in M cells.

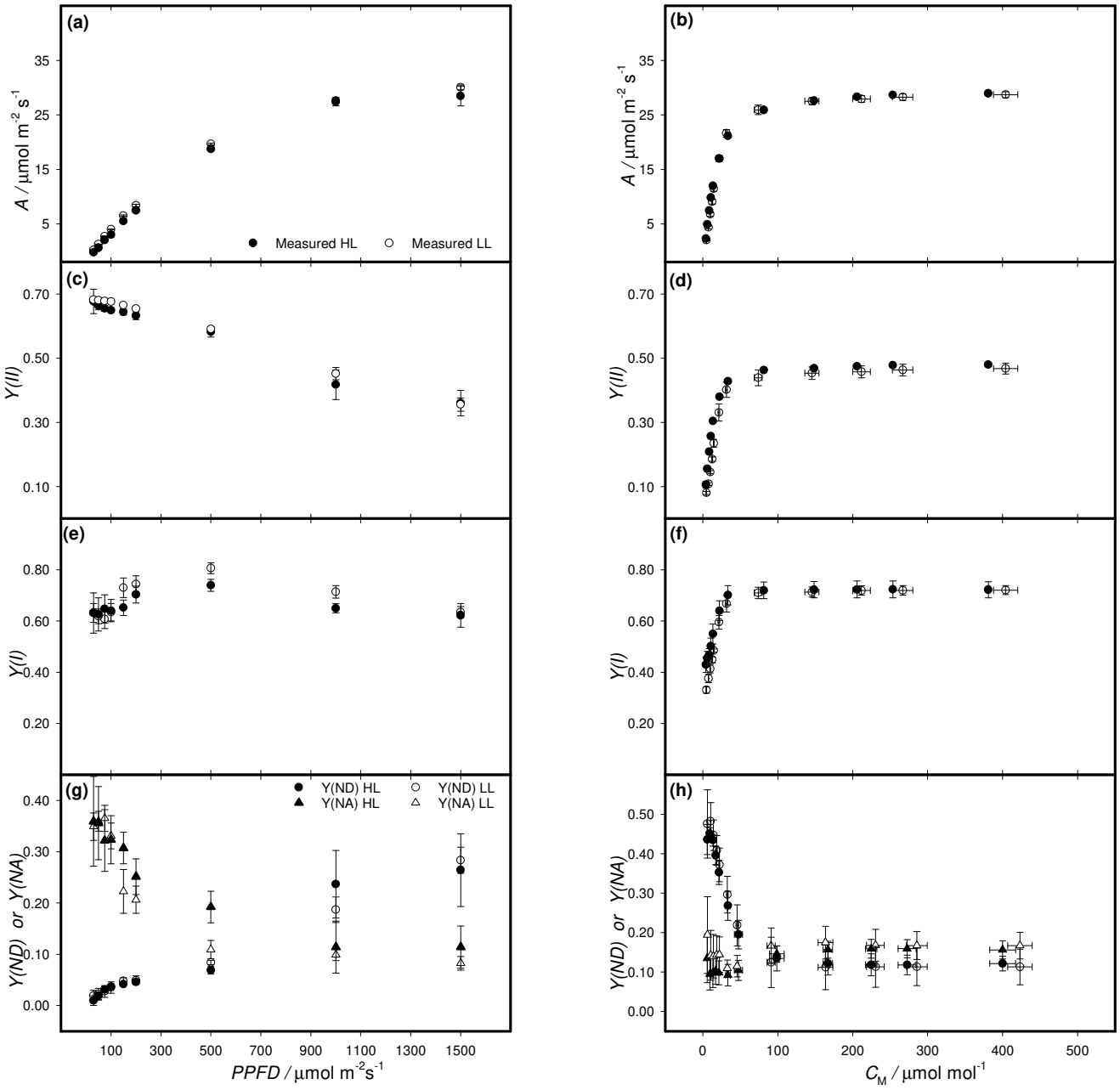

Figure 5. Protein assays. Fluorescent micrographs of pyruvate ortophosphate dikinase (PPDK) localisation on the leaf cross-sections of *S. viridis* grown at low light (LL) and high light (HL). Fluorescence signals are pseudo-coloured: green – PPDK labelled with secondary antibodies conjugated with Alexa Fluor 488; blue – calcofluor white-stained cell walls. BS, bundle sheath cells; M, mesophyll cells. At the bottom, immunodetection of PEP carboxykinase (PEPCK) in leaf protein extracts of *S. viridis* loaded on leaf area basis; *Z. mays* leaf sample was used for positive control. Three biological replicates were loaded for HL and LL plants.

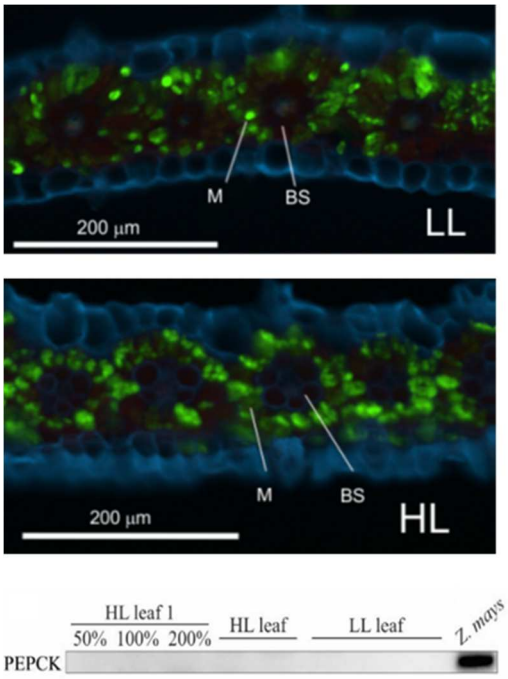

References

Bailey, K.J., Gray, J.E., Walker, R.P. and Leegood, R.C. (2007) Coordinate Regulation of Phosphoenolpyruvate Carboxylase and Phosphoenolpyruvate Carboxykinase by Light and CO2 during C4 Photosynthesis. *Plant Physiol*, **144**, 479-486.

Baker, N.R., Long, S.P. and Ort, D.R. (1988) Photosynthesis and temperature, with particular reference to effects on quantum yield. In *Plants and temperature: Society for Experimental Biology Symposium No XXXXII* (P, L.S. and I, W.F. eds): Company of biologists, pp. 347-375.

Bellasio, C. (2017) A generalised stoichiometric model of C3, C2, C2+C4, and C4 photosynthetic metabolism. *Journal of Experimental Botany*, **68**, 269-282.

Bellasio, C. (2019) A generalised dynamic model of leaf-level C3 photosynthesis combining light and dark reactions with stomatal behaviour. *Photosynth Res*, **141**, 99-118.

Bellasio, C., Beerling, D.J. and Griffiths, H. (2016a) Deriving C_4 photosynthetic parameters from combined gas exchange and chlorophyll fluorescence using an Excel tool: theory and practice. *Plant, Cell & Environment*, **39**, 1164-1179.

Bellasio, C., Beerling, D.J. and Griffiths, H. (2016b) An Excel tool for deriving key photosynthetic parameters from combined gas exchange and chlorophyll fluorescence: theory and practice. *Plant Cell Environ*, **39**, 1180–1197.

Bellasio, C., Burgess, S.J., Griffiths, H. and Hibberd, J.M. (2014) A high throughput gas exchange screen for determining rates of photorespiration or regulation of C4 activity. *Journal of Experimental Botany*, **65**, 3769-3779.

Bellasio, C. and Farquhar, G.D. (2019) A leaf-level biochemical model simulating the introduction of C2 and C4 photosynthesis in C3 rice: gains, losses and metabolite fluxes. *New Phytologist*, **223**, 150-166.

Bellasio, C. and Griffiths, H. (2014a) Acclimation of C4 metabolism to low light in mature maize leaves could limit energetic losses during progressive shading in a crop canopy. *Journal of Experimental Botany*, **65**, 3725-3736.

Bellasio, C. and Griffiths, H. (2014b) Acclimation to Low Light by C4 maize: Implications for Bundle Sheath Leakiness. *Plant Cell Environ*, **37**, 1046-1058.

Bellasio, C. and Griffiths, H. (2014c) The operation of two decarboxylases (NADPME and PEPCK), transamination and partitioning of C4 metabolic processes between mesophyll and bundle sheath cells allows light capture to be balanced for the maize C4 pathway. *Plant Physiol*, **164**, 466-480.

Bellasio, C. and Lundgren, M.R. (2016) Anatomical constraints to C4 evolution: light harvesting capacity in the bundle sheath. *New Phytologist*, **212**, 485–496.

Bellasio, C., Quirk, J., Buckley, T.N. and Beerling, D. (2017) A dynamic hydro-mechanical and biochemical model of stomatal conductance for C4 photosynthesis. *Plant Physiol*, **175**, 104-119.

Berry, J.A. and Farquhar, G.D. (1978) The CO2 concentrating function of C4 photosynthesis: a biochemical model. In *Proceedings of the 4th International Congress on Photosynthesis* (Hall, D., Coombs, J. and Goodwin, T. eds): Biochemical Society, pp. 119-131.

Boesgaard, K.S., Mikkelsen, T.N., Ro-Poulsen, H. and Ibrom, A. (2013) Reduction of molecular gas diffusion through gaskets in leaf gas exchange cuvettes by leaf-mediated pores. *Plant, Cell & Environment*, **36**, 1352-1362.

Boyd, R.A., Gandin, A. and Cousins, A.B. (2015) Temperature Responses of C4 Photosynthesis: Biochemical Analysis of Rubisco, Phosphoenolpyruvate Carboxylase, and Carbonic Anhydrase in Setaria viridis. *Plant Physiol*, **169**, 1850-1861.

Brutnell, T.P., Wang, L., Swartwood, K., Goldschmidt, A., Jackson, D., Zhu, X.-G., Kellogg, E. and Van Eck, J. (2010) Setaria viridis: a model for C4 photosynthesis. *The Plant Cell Online*, **22**, 2537-2544.

Buckley, T.N. and Adams, M.A. (2011) An analytical model of non-photorespiratory CO2 release in the light and dark in leaves of C3 species based on stoichiometric flux balance. *Plant, Cell & Environment*, **34**, 89-112.

Drozak, A. and Romanowska, E. (2006) Acclimation of mesophyll and bundle sheath chloroplasts of maize to different irradiances during growth. *Biochimica et Biophysica Acta (BBA) - Bioenergetics*, **1757**, 1539-1546.

Ermakova, M., Arrivault, S., Giuliani, R., Danila, F., Alonso-Cantabrana, H., Vlad, D., Ishihara, H., Feil, R., Guenther, M., Borghi, G.L., Covshoff, S., Ludwig, M., Cousins, A.B., Langdale, J.A., Kelly, S., Lunn, J.E., Stitt, M., von Caemmerer, S. and Furbank, R.T. (2021a) Installation of C4 photosynthetic pathway enzymes in rice using a single construct. *Plant Biotechnol J*, **doi.org/10.1111/pbi.13487**.

Ermakova, M., Bellasio, C., Fitzpatrick, D., Furbank, R.T., Mamedov, F. and von Caemmerer, S. (2021b) Upregulation of bundle sheath electron transport capacity under limiting light in C4 *Setaria viridis*. *The Plant Journal*, **106**, 1443-1454.

Ermakova, M., Lopez-Calcagno, P.E., Raines, C.A., Furbank, R.T. and von Caemmerer, S. (2019) Overexpression of the Rieske FeS protein of the Cytochrome b6f complex increases C4 photosynthesis in Setaria viridis. *Communications Biology*, **2**, 314.

Ermakova, M., Osborn, H., Groszmann, M., Bala, S., Bowerman, A., McGaughey, S., Byrt, C., Alonso-cantabrana, H., Tyerman, S., Furbank, R.T., Sharwood, R.E. and von Caemmerer, S. (2021c) Expression of a CO2-permeable aquaporin enhances mesophyll conductance in the C4 species Setaria viridis. *Elife*, **10**, e70095.

Evans, J.R., Von Caemmerer, S. and Adams, W.W., III (1991) Ecology of Photosynthesis in Sun and Shade. *Tree Physiology*, **8**, 213-213.

Evans, J.R., von Caemmerer, S., Setchell, B.A. and Hudson, G.S. (1994) The Relationship between Co2 Transfer Conductance and Leaf Anatomy in Transgenic Tobacco with a Reduced Content of Rubisco. *Aust J Plant Physiol*, **21**, 475-495.

Evans, J.R., von Caemmerer, S. and Vogelmann, T.C. (2007) Balancing light capture with distributed metabolic demand during C4 photosynthesis. In *Charting new pathways to C4 rice* (J.E., S., P.L., M. and B., H. eds): IRRI International Rice Research Institute.

Farquhar, G. and Wong, S. (1984) An empirical model of stomatal conductance. *Functional Plant Biology*, **11**, 191-210.

Farquhar, G.D. (1983) On the Nature of Carbon Isotope Discrimination in C4 Species. *Aust J Plant Physiol*, **10**, 205-226.

Farquhar, G.D., von Caemmerer, S. and Berry, J.A. (1980) A biochemical-model of photosynthetic CO2 assimilation in leaves of C3 species. *Planta*, **149**, 78-90.

Furbank, R., Jenkins, C. and Hatch, M. (1990) C4 Photosynthesis: Quantum Requirement, C4 and Overcycling and Q-Cycle Involvement. *Functional Plant Biology*, **17**, 1-7.

Furbank, R.T. (2011) Evolution of the C4 photosynthetic mechanism: are there really three C4 acid decarboxylation types? *Journal of Experimental Botany*, **62**, 3103-3108.

Genty, B., Briantais, J.M. and Baker, N.R. (1989) The relationship between the quantum yield of photosynthetic electron-transport and quenching of chlorophyll fluorescence. *Biochim Biophys Acta*, **990**, 87-92.

Gu, L., Pallardy, S.G., Tu, K., Law, B.E. and Wullschleger, S.D. (2010) Reliable estimation of biochemical parameters from C3 leaf photosynthesis–intercellular carbon dioxide response curves. *Plant, Cell & Environment*, **33**, 1852-1874.

Gutierrez, M., Gracen, V.E. and Edwards, G.E. (1974) Biochemical and cytological relationships in C4 plants. *Planta*, **119**, 279-300.

Hahn, A., Vonck, J., Mills, D.J., Meier, T. and Kühlbrandt, W. (2018) Structure, mechanism, and regulation of the chloroplast ATP synthase. *Science*, **360**, eaat4318.

Henderson, S.A., Von Caemmerer, S. and Farquhar, G.D. (1992) Short-Term Measurements of Carbon Isotope Discrimination in Several C4 Species. *Aust J Plant Physiol*, **19**, 263-285.

Henry, C., Watson-Lazowski, A., Oszvald, M., Griffiths, C., Paul, M.J., Furbank, R.T. and Ghannoum, O. (2019) Sugar sensing responses to low and high light in leaves of the C4 model grass Setaria viridis. *Journal of Experimental Botany*, **71**, 1039-1052.

Ishikawa, N., Takabayashi, A., Noguchi, K., Tazoe, Y., Yamamoto, H., von Caemmerer, S., Sato, F. and Endo, T. (2016) NDH-Mediated Cyclic Electron Flow Around Photosystem I is Crucial for C4 Photosynthesis. *Plant and Cell Physiology*, **57**, 2020-2028.

Ivanov, B., Asada, K., Kramer, D.M. and Edwards, G. (2005) Characterization of photosynthetic electron transport in bundle sheath cells of maize. I. Ascorbate effectively stimulates cyclic electron flow around PSI. *Planta*, **220**, 572-581.

John, C.R., Smith-Unna, R.D., Woodfield, H. and Hibberd, J.M. (2014) Evolutionary convergence of cell specific gene expression in independent lineages of C4 grasses. *Plant Physiol*.

Kanai, R. and Edwards, G.E. (1973) Enzymatic Separation of Mesophyll Protoplasts and Bundle Sheath Cells from C4 Plants. *Naturwissenschaften*, **60**, 157-158.

Kanazawa, A. and Kramer, D.M. (2002) In vivo modulation of nonphotochemical exciton quenching (NPQ) by regulation of the chloroplast ATP synthase. *Proceedings of the National Academy of Sciences*, **99**, 12789-12794.

Karki, S., Lin, H., Danila, F.R., Abu-Jamous, B., Giuliani, R., Emms, D.M., Coe, R.A., Covshoff, S., Woodfield, H. and Bagunu, E. (2020) A role for neutral variation in the evolution of C4 photosynthesis. *bioRxiv*.

Klughammer, C. and Schreiber, U. (1994) An Improved Method, Using Saturating Light-Pulses, for the Determination of Photosystem-I Quantum Yield Via P700+-Absorbency Changes at 830 Nm. *Planta*, **192**, 261-268.

Klughammer, C. and Schreiber, U. (2008) Saturation Pulse method for assessment of energy conversion in PS I. *PAM Application notes*, **1**, 3.

Kramer, D.M. and Evans, J.R. (2011) The Importance of Energy Balance in Improving Photosynthetic Productivity. *Plant Physiol*, **155**, 70-78.

Kromdijk, J., Griffiths, H. and Schepers, H.E. (2010) Can the progressive increase of C4 bundle sheath leakiness at low PFD be explained by incomplete suppression of photorespiration? *Plant Cell Environ*, **33**, 1935-1948.

Kromdijk, J., Ubierna, N., Cousins, A.B. and Griffiths, H. (2014) Bundle-sheath leakiness in C4 photosynthesis: a careful balancing act between CO2 concentration and assimilation. *Journal of Experimental Botany*, **65**, 3443-3457.

Long, S.P. (1993) The significance of light-limited photosynthesis to crop canopy carbon gain and productivity - a theoretical analysis. In *Photosynthesis: Photoreactions to Plant Productivity* (Abrol, Y.P., Mohanty, P. and Govindjee eds). New Delhi: Oxford & IBH publishing, pp. 547 - 560.

Maai, E., Nishimura, K., Takisawa, R. and Nakazaki, T. (2020a) Diurnal changes in chloroplast positioning and photosynthetic traits of C4 grass finger millet. *Plant Production Science*, 1-13.

Maai, E., Nishimura, K., Takisawa, R. and Nakazaki, T. (2020b) Light stress-induced chloroplast movement and midday depression of photosynthesis in sorghum leaves. *Plant Production Science*, **23**, 172-181.

Mallmann, J., Heckmann, D., Brautigam, A., Lercher, M.J., Weber, A.P.M., Westhoff, P. and Gowik, U. (2014) The role of photorespiration during the evolution of C4 photosynthesis in the genus Flaveria. *Elife*, **3**, 10.7554/eLife.02478.

McQualter, R.B., Bellasio, C., Gebbie, L., Petrasovits, L.A., Palfreyman, R., Hodson, M., Plan, M., Blackman, D., Brumbley, S. and Nielsen, L. (2016) Systems biology and metabolic modelling unveils limitations to polyhydroxybutyrate accumulation in sugarcane leaves; lessons for C4 engineering. *Plant Biotechnol J*, **14**, 567–580.

Osmond, C. (1974) Carbon reduction and photosystem II deficiency in leaves of C4 plants. *Aust J Plant Physiol*, **1**, 41-50.

Pengelly, J.J.L., Sirault, X.R.R., Tazoe, Y., Evans, J.R., Furbank, R.T. and von Caemmerer, S. (2010) Growth of the C4 dicot Flaveria bidentis: photosynthetic acclimation to low light through shifts in leaf anatomy and biochemistry. *Journal of Experimental Botany*, **61**, 4109-4122.

Peterson, R.B., Schultes, N.P., McHale, N.A. and Zelitch, I. (2016) Evidence for a Role for NAD(P)H Dehydrogenase in Concentration of CO₂ in the Bundle Sheath Cell of <em>Zea mays</em&gt. *Plant Physiol*, **171**, 125.

Pick, T.R., Brautigam, A., Schluter, U., Denton, A.K., Colmsee, C., Scholz, U., Fahnenstich, H., Pieruschka, R., Rascher, U., Sonnewald, U. and Weber, A.P.M. (2011) Systems Analysis of a Maize Leaf Developmental Gradient Redefines the Current C-4 Model and Provides Candidates for Regulation. *Plant Cell*, **23**, 4208-4220.

Porra, R.J., Thompson, W.A. and Kriedemann, P.E. (1989) Determination of accurate extinction coefficients and simultaneous equations for assaying chlorophylls a and b extracted with four different solvents: verification of the concentration of chlorophyll standards by atomic absorption spectroscopy. *Biochimica et Biophysica Acta (BBA) - Bioenergetics*, **975**, 384-394.

Rogowski, P., Wasilewska-Dębowska, W., Krupnik, T., Drożak, A., Zienkiewicz, M., Krysiak, M. and Romanowska, E. (2019) Photosynthesis and organization of maize mesophyll and bundle sheath thylakoids of plants grown in various light intensities. *Environmental and Experimental Botany*, **162**, 72-86.

Romanowska, E., Drozak, A., Pokorska, B., Shiell, B.J. and Michalski, W.P. (2006) Organization and activity of photosystems in the mesophyll and bundle sheath chloroplasts of maize. *J Plant Physiol*, **163**, 607-618.

Sage, R.F. (2017) A portrait of the C4 photosynthetic family on the 50th anniversary of its discovery: species number, evolutionary lineages, and Hall of Fame. *Journal of experimental botany*, **68**, e11-e28.

Sagun, J.V., Badger, M.R., Chow, W.S. and Ghannoum, O. (2021) Mehler reaction plays a role in C3 and C4 photosynthesis under shade and low CO2. *Photosynth Res*.

Sales, C.R.G., Ribeiro, R.V., Hayashi, A.H., Marchiori, P.E.R., Silva, K.I., Martins, M.O., Silveira, J.A.G., Silveira, N.M. and Machado, E.C. (2018) Flexibility of C4 decarboxylation and photosynthetic plasticity in sugarcane plants under shading. *Environmental and Experimental Botany*, **149**, 34-42.

Schlüter, U., Bräutigam, A., Droz, J.-M., Schwender, J. and Weber, A.P.M. (2019) The role of alanine and aspartate aminotransferases in C4 photosynthesis. *Plant Biology*, **21**, 64-76.

Schlüter, U. and Weber, A.P.M. (2020) Regulation and Evolution of C4 Photosynthesis. *Annual Review of Plant Biology*, **71**, null.

Schreiber, U., Schliwa, U. and Bilger, W. (1986) Continuous recording of photochemical and non-photochemical chlorophyll fluorescence quenching with a new type of modulation fluorometer. *Photosynth Res*, **10**, 51-62.

Sharwood, R.E., Sonawane, B.V. and Ghannoum, O. (2014) Photosynthetic flexibility in maize exposed to salinity and shade. *Journal of experimental botany*, **65**, 3715-3724.

Sonawane, B.V., Sharwood, R.E., Whitney, S. and Ghannoum, O. (2018) Shade Compromises the Photosynthetic Efficiency of NADP-ME less than PEP-CK and NAD-ME C4 Grasses. *Journal of Experimental Botany*, **69**, 3053–3068.

Takabayashi, A., Kishine, M., Asada, K., Endo, T. and Sato, F. (2005) Differential use of two cyclic electron flows around photosystem I for driving CO2-concentration mechanism in C4 photosynthesis. *P Natl Acad Sci USA*, **102**, 16898-16903.

Terashima, I., Fujita, T., Inoue, T., Chow, W.S. and Oguchi, R. (2009) Green Light Drives Leaf Photosynthesis More Efficiently than Red Light in Strong White Light: Revisiting the Enigmatic Question of Why Leaves are Green. *Plant and Cell Physiology*, **50**, 684-697.

Ubierna, N., Gandin, A., Boyd, R.A. and Cousins, A.B. (2017) Temperature response of mesophyll conductance in three C4 species calculated with two methods: 18O discrimination and in vitro Vpmax. *New Phytologist*, **214**, 66–80.

Ubierna, N., Sun, W., Kramer, D.M. and Cousins, A.B. (2013) The Efficiency Of C4 Photosynthesis Under Low Light Conditions In Zea mays, Miscanthus X giganteus And Flaveria bidentis. *Plant, Cell & Environment*, **36**, 365-381.

Vollmar, M., Schlieper, D., Winn, M., Büchner, C. and Groth, G. (2009) Structure of the c14 Rotor Ring of the Proton Translocating Chloroplast ATP Synthase. *J Biol Chem*, **284**, 18228-18235.

von Caemmerer, S. (2000) *Biochemical models of leaf Photosynthesis* Collingwood: CSIRO Publishing.

von Caemmerer, S., Evans, J., Cousins, A., Badger, M. and Furbank, R.T. (2008) C 4 photosynthesis and CO 2 diffusion. In *Charting new pathways to C4 rice*: World Scientific, pp. 95-115.

von Caemmerer, S. and Furbank, R.T. (2003) The C4 pathway: an efficient CO2 pump. *Photosynth Res*, **77**, 191-207.

Ward, D.A. and Woolhouse, H.W. (1986) Comparative effects of light during growth on the photosynthetic properties of NADP-ME type C4 grasses from open and shaded habitats. I. Gas exchange, leaf anatomy and ultrastructure*. *Plant, Cell & Environment*, **9**, 261-270.

Yamada, M., Kawasaki, M., Sugiyama, T., Miyake, H. and Taniguchi, M. (2009) Differential Positioning of C4 Mesophyll and Bundle Sheath Chloroplasts: Aggregative Movement of C4 Mesophyll Chloroplasts in Response to Environmental Stresses. *Plant and Cell Physiology*, **50**, 1736-1749.

Yin, X., Struik, P.C., Romero, P., Harbinson, J., Evers, J.B., Van Der Putten, P.E.L. and Vos, J.A.N. (2009) Using combined measurements of gas exchange and chlorophyll fluorescence to estimate parameters of a biochemical C3 photosynthesis model: a critical appraisal and a new integrated approach applied to leaves in a wheat (Triticum aestivum) canopy. *Plant, Cell & Environment*, **32**, 448-464.

Yin, X., Van Oijen, M. and Schapendonk, A. (2004) Extension of a biochemical model for the generalized stoichiometry of electron transport limited C3 photosynthesis. *Plant, Cell & Environment*, **27**, 1211-1222.

Yin, X.Y. and Struik, P.C. (2012) Mathematical review of the energy transduction stoichiometries of C4 leaf photosynthesis under limiting light. *Plant Cell Environ*, **35**, 1299-1312.